

GT2011-46369

The Aero-thermal Performance of a Cooled Winglet Tip in a High Pressure Turbine Cascade

Chao Zhou*

State Key Laboratory for Turbulence and
Complex Systems, College of Engineering,
Peking University,
Beijing, China

Howard Hodson

Whittle Laboratory
Department of Engineering,
University of Cambridge, UK

Ian Tibbott and Mark Stokes

Rolls-Royce plc,
Derby
UK

ABSTRACT

The aero-thermal performance of a winglet tip with cooling holes on the tip and on the blade surface near the tip is reported in this paper. The investigation was based on a high pressure turbine cascade. Experimental and numerical methods were used. The effects of the coolant mass flow rate are also studied.

Because the coolant injection partially blocks the tip leakage flow, more passage flow is turned by the blade. As a result, the coolant injection on the winglet tip reduces the deviation of the flow downstream of the cascade due to the tip leakage flow. However, the tip leakage loss increases slightly with the coolant mass flow ratio.

Both the CFD tools and experiments using the Amonia-Diazo technique were used to determine the cooling effectiveness. On the blade pressure side surface, low cooling effectiveness appears around the holes due to the lack of the coolant from the cooling hole or the lift-off of the coolant from the blade surface when the coolant mass flow is high. The cooling effectiveness on the winglet tip is a combined effect of the coolant ejected from all the holes.

On the top of the winglet tip, the average cooling effectiveness increases and the heat load decreases with increasing coolant mass flow. Due to its large area, the cooled winglet tip has a higher heat load than an uncooled flat tip at engine representative coolant mass flow ratio. Nevertheless, the heat flux rate per unit area of the winglet is much lower than that of an uncooled flat tip.

INTRODUCTION

In unshrouded high pressure axial turbines, the tip leakage flow results in an undesirable loss of efficiency. It can also cause excessively high metal temperatures on the blade tip. Obtaining a good aero-thermal performance of the blade tip represents a major challenge for turbine designers.

It is generally believed that a reduction of the tip leakage mass flow rate will result in a reduction of the tip leakage loss.

* The work presented in this paper was carried out in the Whittle Laboratory, Cambridge University.

Email:chao.zhou@cantab.net

With a winglet on the blade tip, the driving pressure difference of the tip leakage flow can be reduced. Thus, the tip leakage mass flow rate and the tip leakage loss may decrease. Schabowski and Hodson [1] studied the aerodynamic performance of several squealer tips and winglet-cavity tips in a linear cascade. Their optimum winglet-cavity tip produced a lower loss than the squealer tips and offered a 37% reduction in the loss vs. tip gap slope compared to a flat tip. Yaras and Sjolander [2] investigated a winglet tip in a low speed linear cascade at a tip gap of 2.4% of blade span. They obtained a 10 percent reduction in the tip leakage loss by using the winglet tip. They found that the pressure side winglet reduced the discharge coefficient of the tip leakage flow, while the suction side winglet reduced the driving pressure difference across the tip.

A test by Liu et al. [3] using a low aspect ratio turbine showed that the double winglet tip improved the stage efficiency by 0.6 percent at a relatively large tip gap of 3 percent of blade span. Harvey [4] reported an investigation of two winglet tips in a research turbine. The turbine test showed that the winglet tips provided no improvement in stage efficiency. It was concluded that if these winglet tips did reduce the tip leakage flow over the tip, then it must have been at the expense of increased losses in the passage flow due to the use of the winglet tip.

In a single stage axial flow turbine facility, Dey and Camei [5] found that a tip with a pressure side winglet would reduce the loss. A tip with a suction side winglet pushed the core of the tip vortex further away from the blade suction side, but did not improve the efficiency. Harvey et al. [6] studied a winglet-cavity tip and several shrouded tips in a cool flow high speed engine rig. The results showed that the winglet was as good as a shrouded tip with two fins in terms of reducing the tip leakage loss (45% less than a flat tip).

There are only a few open publications that studied the thermal performance of winglet tips. In a linear cascade, Papa et al. [7] found that the use of the winglet reduced the heat transfer coefficient on the flat tip and the suction side squealer tip. O'Dowd et al. [8] studied the thermal performance of a winglet tip at engine representative conditions in a transonic linear cascade. Compared to the flat tip, the winglet had a 13% higher average Nusselt number. It also had nearly 2.4 times the

surface area, which means that the average heat load for the winglet was nearly 2.7 times greater for the winglet than the flat tip.

Cooling air is often used to improve the thermal performance of the tips in high pressure turbines. Tip coolant injection was observed to be able to partially block the tip leakage flow by, for example, Hohlfeld et al. [9] and Zhou and Hodson [10].

The effects of the coolant injection on a cavity tip and a suction side squealer tip were studied by Hofer et al. [11] and Hofer and Arts [12] in a linear cascade. The coolant was ejected from both the top of the tip and the blade pressure side surface. They found that the impact of the coolant on the overall loss was marginal. For the cavity tip, the maximum reduction in the tip leakage loss was 6.4% at low Mach numbers. At high Mach number, the leakage loss increased by a maximum of 5.7% due to the coolant. The tip leakage loss of the cooled suction side squealer tip changed only slightly with coolant injection.

Kim and Metzger [13] studied the thermal performance of 2D blade tip cooling models using experiments. They found that with the injection of the coolant, the heat transfer coefficient on the blade tip increased. So, if the temperature of the coolant was not low enough, the injection would actually increase the heat load on the tip. The blowing ratio affected the performance of the tip cooling air. If the blowing ratio was too low, there would not be enough coolant; if the blowing ratio was too high, the coolant would lift off from the blade tip surface. Both of these cases resulted in a reduction in the cooling effectiveness on the blade tip. In a low speed linear cascade, Newton et al [14] found that as the blowing ratio increased from 0.74 to 0.99, the thermal performance of a cooled flat tip became worse.

Christophel et al [15][16] found that coolant ejected from dust holes on the tip improved the thermal performance near the leading edge of the tip, especially at small tip gaps. The effects of coolant injection from both the tip and the pressure side near tip region were studied by Ahn et al. [17] using a flat tip and a cavity tip. In general, the cooling effectiveness increased as the blowing ratio increased on each of the tips. Coolant injection on the pressure side created more cooling on a flat tip than that on a cavity tip. They found that the effect of the size of the tip gap on the tip cooling effectiveness was small.

In a transonic cascade, O'Dowd et al. [24] studied the thermal performance of a flat tip. It was found that the adiabatic wall recovery temperature was higher near the leading edge of the tip. Shock waves were observed from the mid-chord to the trailing edge of the blade tip. The adiabatic wall temperature on the blade tip was affected by the shockwave pattern within the tip gap. Wheeler et al. [25] compared the heat transfer at high speed and low speed on a plain tip. Increasing the Mach number reduced the size of the separation zone near the pressure side inlet of the tip gap. Shock waves appear inside the tip gap when the Mach number increases. The increase of the Mach number reduced the turbulence viscosity inside the tip gap. This reduced the heat flux on the blade tip. Compared with the high speed case, the heat load obtained in the low speed study was higher. In cases where squealers are used, the flow

patterns are likely to be more similar at both high speed and low speed, because choking tends to occur over the suction side squealer (Chen et al. [27]).

According to the authors' knowledge, there is no open publication that studied the aero-thermal performance of a winglet tip with coolant injection. The objectives of the paper are to investigate the effects of the coolant on both the aerodynamic and the thermal performance of a winglet tip and to investigate the effects of the coolant mass flow ratio. The flow pattern downstream of the cascade, the tip leakage loss and thermal parameters such as cooling effectiveness, Nusselt number were also studied.

NOMENCLATURE

C	Blade chord
C_p	Surface static pressure coefficient = $(p_{01}-p)/(p_{01}-p_2)$
$C_{p,0}$	Stagnation pressure loss coefficient = $(p_{01}-p_0)/(p_{01}-p_2)$
C_{iw}	Concentration of tracer gas on impermeable wall
C_{jet}	Concentration of tracer gas in the jet
C_∞	Concentration of tracer gas in local free stream flow
h	Heat transfer coefficient $h = q/(T_{aw} - T_w)$
k_{air}	Thermal conductivity of the air
M_c	Coolant mass flow ratio
$M_{c,ER}$	Engine representative coolant mass flow ratio
$NHFR$	Net Heat Flux Reduction
Nu	Nusselt Number = hC/k_{air}
p	Static pressure
p_0	Stagnation pressure
q	Local heat flux per unit area
Q	Overall heat flux
Re	Reynolds number $Re = \rho VC/\mu$
T	Temperature
T_0	Stagnation temperature
T_{aw}	Adiabatic wall temperature
T_w	Wall temperature
V	Velocity
$Y_{p-total}$	Total loss coefficient
Y_{p-tip}	Tip leakage loss coefficient
ρ	Density
η	Cooling Effectiveness $\eta = (T_{aw} - T_{01})/(T_{0c} - T_{01})$
η_{iw}	Impermeable wall concentration
τ	Tip gap height
μ	Dynamic viscosity
σ	Contraction coefficient (=Unblocked height at the vena-contracta / tip gap)
Θ_E	Non-dimensional engine temperature

Subscripts

1	Cascade inlet free stream
2	Cascade exit
3	Mixed-out exit condition

EXPERIMENTAL METHODS

A low speed linear cascade was built based on the near tip section of a high pressure turbine rotor. The cascade was placed at the exit of the wind tunnel and exhausted to atmospheric

pressure. The free stream inlet turbulence intensity of the wind tunnel is about 0.5%. Key parameters of the cascade are presented in Table 1.

Number of Blades	6
Chord (C)	200mm
Pitch/Chord ratio (S/C)	0.9
Axial Chord (C_x)	124mm
Aspect Ratio (Blade Height/Chord)	2.25
Design Inlet Flow Angle	-41°
Design Exit Flow Angle	68.5°
Re_{exit}	4.0×10^5

Table 1 Parameters of the Cascade

Fig. 1 shows the overall layout of the cascade. It has boundary layer bleed slots upstream of the blade leading edge. A tailboard is used at the trailing edge of the top blade to adjust the periodicity of the cascade. During all of the experiments, the four central blades have the same size of the tip gap. The third blade from the top is cooled. Static pressure tappings are used in the coolant plenum. The coolant mass flow rate is measured by a flow meter with an accuracy of better than 1%. The other three tips are uncooled winglet tips for all of the experiments. The two end blades have small fixed tip gaps of less than 0.5mm (0.25%C) to allow the movement of the traversable casing endwall. The traversable casing endwall is moved in the tangential direction by a stepper motor.

The inlet boundary layer of the cascade is measured with a flattened boundary layer pitot probe, which has a width of 1.8 mm and a thickness of 0.6 mm. The inlet boundary layer probe was traversed with the movable endwall to measure the inlet boundary at 35% axial chord upstream of the blade leading edge. A row of 14 static pressure tappings are placed on the movable endwall at different axial locations. By traversing the endwall in the pitchwise direction, the static pressure distributions on the endwall are measured.

On the hub wall of the cascade, five static pressure tappings are located at 50 percent of an axial chord upstream of the blade leading edge and five others are placed at 63 percent of an axial chord downstream of the blade trailing edge. Three pitot tubes, which are located at 50 percent of an axial chord upstream of the cascade, measure the free stream inlet stagnation pressure of the cascade. The temperature of the flow is measured by a thermocouple near the exit of the wind tunnel.

A calibrated 90 degree pyramid five-hole probe is traversed on a plane that is located 45 percent of the axial chord downstream of the blade trailing edge to measure the loss of the third blade from the top. The diameter of the five-hole probe is 3.25mm. During the traverse, when the probe was closet to the wall, the gap between the five-hole probe and the endwall is 1.5mm. A total of 1334 points are used to cover an area of 228mm in the pitchwise direction (1.27 pitches) and up to 140mm away from the endwall in spanwise direction. The losses are evaluated over one pitch.

The distribution of the cooling effectiveness of the winglet tip is obtained by using the Ammonia - Diazo technique, which uses the analogy between the heat and mass transfer. The ammonia gas was mixed with the coolant. It reacts with the

chemicals on the diazo paper, which is attached to the blade tip. Depending on the concentration of ammonia, the chemical reaction leaves traces of different darkness on the diazo paper, from which the cooling effectiveness is derived. The Ammonia - Diazo technique used in the current study is the same as that used by Friedrichs et al. [19].

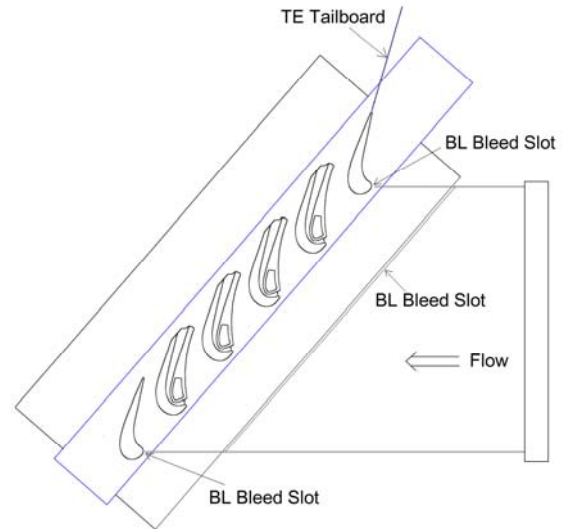


Fig. 1 Layout of Cascade

To calibrate the Ammonia-Diazo film cooling experiment, a reference experiment is performed in parallel to the main experiment. In the reference experiment, a calibration strip is produced by mixing the seeded coolant gas with the free stream air from the wind tunnel in known ratios. All the dependencies are automatically taken into account, as the calibration strip is exposed to the representative mixtures for the same amount of time as the main experiment.

Analogous to the adiabatic cooling effectiveness, an impermeable wall effectiveness based on concentration measurements can be defined as

$$\eta_{iw} = \frac{C_{iw} - C_{\infty}}{C_{jet} - C_{\infty}} \quad \text{Eq. 1}$$

where C_{iw} is the concentration of the trace gas on the impermeable wall, C_{jet} is the concentration of the trace gas of the jet and C_{∞} is the concentration of the gas of the local free stream flow.

The conditions for the use of the analogy between heat and mass transfer in cooling investigation have been reviewed by Shadid and Eckert [26]. When they are met, the impermeable wall concentration field is similar to the adiabatic wall temperature field and the two effectiveness parameters are equal:

$$\eta_{iw} = \eta \quad \text{Eq. 2}$$

where η_{iw} is the impermeable wall concentration and η is the cooling effectiveness.

In the present experiments only the coolant is seeded with ammonia. The free stream concentration therefore corresponds to a value of 0%. With the relative coolant concentration in the plenum being 100%, the measured relative concentration values

are equivalent to the adiabatic cooling effectiveness. Therefore in this case:

$$\eta_{iw} = \eta = \frac{C_{iw}}{C_{jet}} = C_{rel} \quad \text{Eq. 3}$$

Fig. 2 shows the geometry of the cooled winglet tip. Winglets exist on both the pressure side and the suction side of the tip. The edge of the pressure side winglet leans towards the flow passage. A gutter is located almost along the camber line of the blade. A cavity is located on the pressure side winglet. The depth of the gutter and the cavity is 4%C. The suction side winglet is plain. The cooling holes are located on the near tip region of the blade surface and in the gutter and the cavity of the winglet tip. No cooling hole is located on the top surface of the winglet tip.



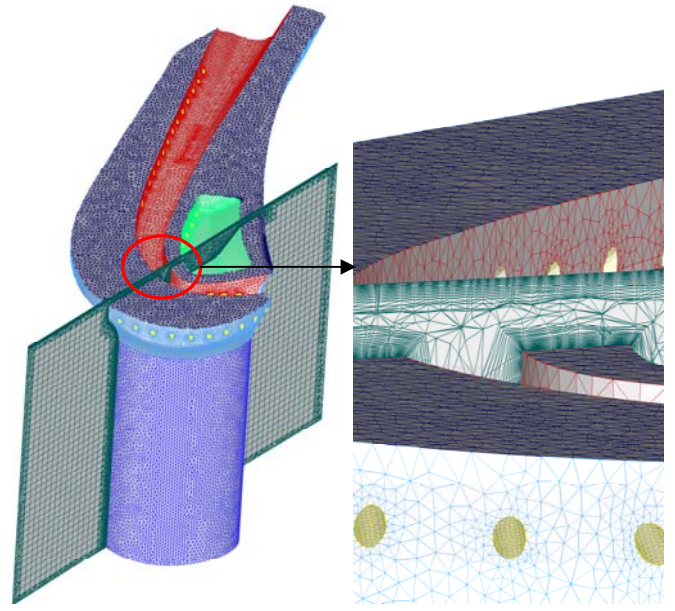
Fig. 2 Geometry of Cooled Winglet Tip

NUMERICAL METHODS

The commercial code Fluent 6.3 was used to solve the RANS equations. The Spalart-Allmaras turbulence model was used. ICEMCFD was used to build the meshes. Unstructured meshes were built for the cooled winglet tips as shown in Fig. 3, because the cooled winglet tip geometry is too complex to be meshed with structured mesh in the time that was available. Nevertheless, this mesh is adequate for the current study as shown later in this paper.

The hexa-core was used in the main flow passage of the mesh as shown in Fig. 3(a). Prism meshes were used on all of the surfaces to capture the flow pattern near all the walls, even for the inner surfaces of the cooling holes. An average Y^+ of about 1 was achieved in the numerical results. The maximum Y^+ is about 6. In a grid dependency study for a similar problem (Zhou and Hodson [10]), the variation of the tip leakage loss was less than 0.6% of the loss when the average Y^+ on the blade tip was changed from less than 1 to nearly 10. According to Zhou and Hodson [18], the variation of the heat transfer coefficient is less than 10% when the average tip Y^+ changes from about 0.5 to nearly 6.

Periodic boundary conditions were applied to a single blade to simulate a row of blades. The inlet of the computational domain is located 1.2 axial chords upstream the blade leading edge. The free stream stagnation pressure of 660Pa-gauge was applied at the inlet of the cascade. No boundary layer was applied at the inlet because the boundary layer bleed slot of the cascade is also located at this position in the experiment. The boundary layer develops as the flow enters the test section.



(a) Over View

(b) Mesh in Tip Gap

Fig. 3 Mesh of Cooled Winglet Tip, $\tau=1.9\%C$

The predicted boundary layer at 35% axial chord upstream of the blade leading edge was compared with the measurement. The CFD predicted a boundary layer with a 99% thickness of 2%C and a shape factor of 1.3. The measurement at this location yielded a 99% thickness of 2.5%C and a shape factor of 1.26. The displacement thickness is predicted to be 0.26%C and is 0.31%C in the experiment.

The outlet of the computational domain is 1.6 axial chords downstream of the trailing edge of the blade. Atmospheric pressure (0 Pa-gauge) was applied at the exit of the computational domain. A stagnation pressure was defined at the inlet of the coolant plenum. The Reynolds number was 4.0×10^5 based on the blade chord and the exit conditions. No slip boundary conditions were applied to all walls. A symmetry boundary condition was used for the 'hub' of the computational domain.

LOSS DEFINITION

The total mixed-out loss was calculated by assuming that the cascade exit flow was fully mixed out at constant area. The effective span used in the calculation is 1.34 Chord.

The total loss coefficient is defined as

$$Y_{p_total} = (p_{01_ref} - p_{03}) / (p_{01_ref} - p_3) \quad \text{Eq. 4}$$

where p_{01_ref} is the reference stagnation pressure, p_{03} is the stagnation pressure at the mixed-out exit plane, and p_3 is the static pressure at the mixed-out exit plane.

For the loss calculation of the cooled tips, the stagnation pressure of the coolant should be taken into account. So, the reference stagnation pressure p_{01_ref} is defined as

$$p_{01_ref} = (\dot{m}_m \cdot p_{01} + \dot{m}_c \cdot p_{0c}) / (\dot{m}_m + \dot{m}_c) \quad \text{Eq. 5}$$

where \dot{m}_m is the mass flow rate at the inlet of the cascade, and \dot{m}_c is the mass flow rate of the coolant, p_{01} is the free stream stagnation pressure at the cascade inlet, and p_{0c} is the average stagnation pressure at the coolant inlet. For uncooled cases, $\dot{m}_c = 0$.

The coolant mass flow ratio is defined as

$$M_c = \dot{m}_c / \dot{m}_m \quad \text{Eq. 6}$$

where \dot{m}_c is the coolant mass flow rate, \dot{m}_m is the cascade inlet mass flow rate based on an effective span.

The tip leakage loss was obtained by subtracting the profile loss from the total mixed-out loss. The profile loss is obtained as:

$$Y_{p_profile} = (p_{01} - p_{03_prof}) / (p_{01} - p_3) \quad \text{Eq. 7}$$

where p_{03_prof} is the mixed-out stagnation pressure coefficient at the mid-span. The profile loss coefficient of the experiment is 0.032 ± 0.002 and the predicted value is 0.046. The blade profile loss is over predicted because in the numerical simulation, the flow is fully turbulent, while in real case, boundary layer transition happens on the blade surface. A laminar boundary layer produces a lower loss than the turbulent boundary layer. The uncertainty of the tip leakage loss obtained in the experiments was better than 0.002.

RESULTS AND DISCUSSIONS

Blade Surface Static Pressure Coefficient

Fig. 4 shows the predicted static pressure coefficient on the blade surface. The static pressure coefficient is plotted against the axial chord in Fig. 4(a) and against the tangential chord in Fig. 4(b).

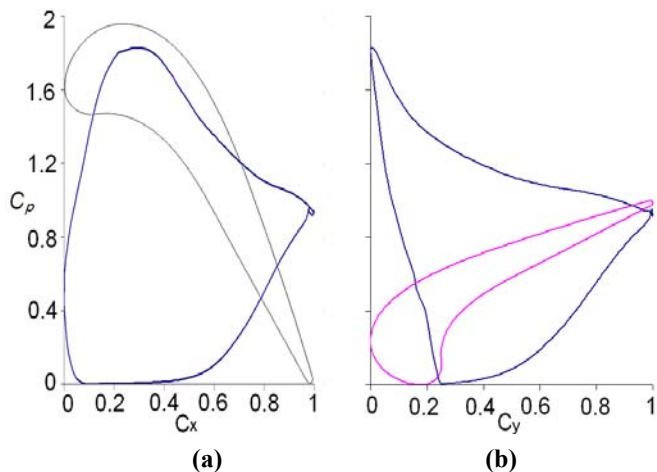


Fig. 4 Mid-span C_p distribution, CFD

Fig. 4(a) shows that the static pressure coefficients on the pressure side surface of the blade from about 10 percent of the

axial chord to about 40 percent of the axial chord are almost zero. After 40% of the axial chord, the flow accelerates up to the trailing edge on the blade pressure side. On the suction side of the blade, the flow accelerates to around 30% of the axial chord and then gradually decelerates towards the trailing edge. Fig. 4(b) gives a better presentation of the driving pressure difference of the tip leakage flow, because the direction of the tip leakage flow is closer to the axial direction rather than the tangential direction.

Coolant Static Pressures

Fig. 5 shows the distribution of the static pressure coefficient (C_p) on the surfaces of the internal coolant passage at the engine representative coolant mass flow ratio ($M_{c,ER}$). The coolant is fed from the coolant plenum. The static pressure coefficients in the plenum are quite uniform and are low. The coolant is ejected from the coolant plenum via the coolant pipes. From the leading edge to about the mid-chord, the coolant pipes are connected directly to the coolant plenum. Near the trailing edge of the tip, two tubes are used to provide the coolant to each of the winglets. The coolant enters the coolant tubes from the coolant plenum. It is then injected into the blade passage via the coolant pipes. The coolant accelerates into the coolant pipes or the coolant tubes, so the static pressures in the coolant pipes and in the coolant tubes are lower than that in the coolant plenum.

The static pressure near area 'A' in Fig. 5 is low, because the coolant accelerates into the coolant tube of the pressure side winglet. As a result, the driving pressure differences for the coolant in the cooling holes near area 'A' are also small, resulting in low coolant mass flow rates for these holes. The static pressure at the inlet of the cooling holes in area 'B' of Fig. 5 is much higher than that of the holes located in area 'A'. As the exit static pressure is similar for the holes located in areas 'A' and 'B', the driving pressure differences, as well as the coolant mass flow rates are larger for the coolant pipes located in area 'B' than those in area 'A'. This has an effect on the thermal performance of the blade tip, which will be presented later in this paper.

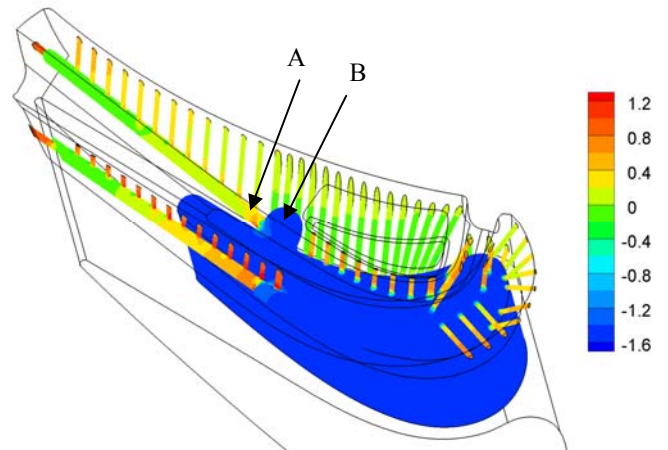


Fig. 5 C_p of Internal Cooling Configuration, $M_{c,ER}$, $\tau = 1.9\%C$, CFD

Flow downstream of Cascade

The experimental spanwise distribution of the pitchwise averaged flow fields of the winglet tips at 45% axial chord downstream of the cascade are shown in Fig. 6. The effects of coolant were studied at a tip gap of 1.9%C. The case of uncooled winglet tip at 1.25%C is also presented. The coolant injection partially blocks the flow that enters the tip gap from the pressure side of the tip gap, so more flow is turned by the blade. This changes the flow pattern downstream of the cascade near the endwall.

Fig. 6(a) shows the pitchwise mass averaged stagnation pressure coefficient relative to the value at the midspan. At the coolant mass flow ratio of 48% $M_{c,ER}$, the distribution of the stagnation pressure coefficient slightly improves. At the engine representative coolant mass flow ratio ($M_{c,ER}$), the stagnation pressure coefficient reduces near the endwall but increases from 20% to 40% of a chord in the spanwise direction. Fig. 6 (b) shows the momentum based yaw angle deviation. The injection of the coolant reduces the deflection due to the tip leakage flow. This effect is larger at a larger coolant mass flow ratio. The deflection of the downstream flow angle reduces by about 9 degrees near the endwall at the engine representative coolant mass flow ratio.

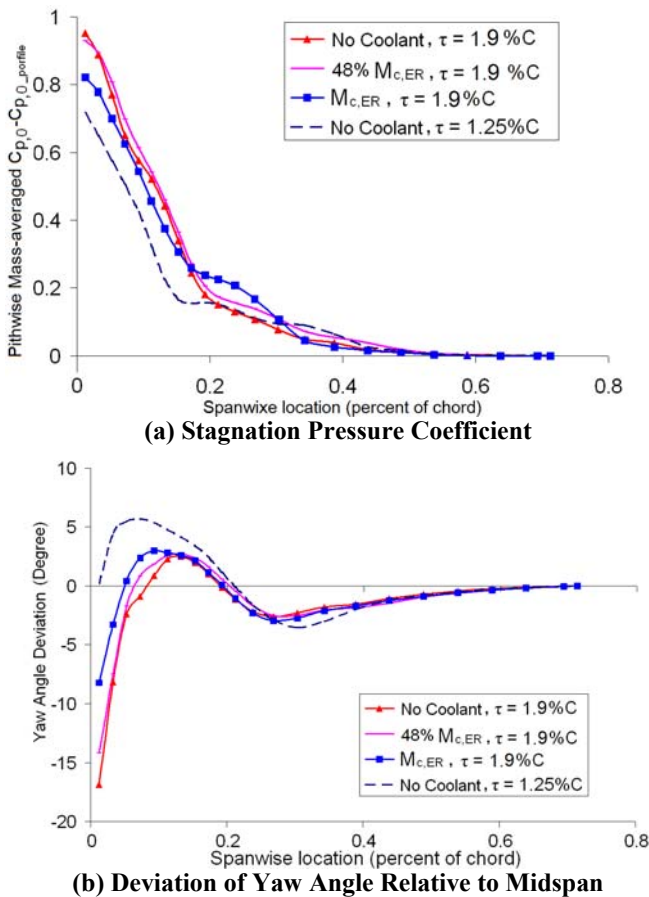


Fig. 6 Effects of Coolant to Flow Field, $\tau=1.9\%C$ 45% Axial Chord Downstream Cascade, Exp.

On a large scale rotational rig, Dey [21] found that a coolant mass flow ratio of 0.3% was not high enough to cause a significant reduction of the tip leakage loss. On the same rig, Rao and Camci [22] obtained a significant reduction of the stagnation pressure deficit at the exit of the stage by ejecting coolant from the top of a flat tip. At a tip gap of 1.4% of the span, when ejecting the tip coolant at mass flow ratios from 0.41% to 0.72%, the distribution of the stagnation pressure coefficient downstream the blade row was similar to the case when the tip gap was 0.72% of the span without coolant ejection.

In the current study, the improvement of downstream flow field is small at 48% $M_{c,ER}$. At the engine representative coolant mass flow ratio ($M_{c,ER}$), the distribution of the stagnation pressure downstream of the cascade improves, but it is still worse than that of the uncooled winglet tip at the gap of 1.25%C.

Effect of Coolant Flow on Tip Leakage Loss

Although coolant injection improves the flow distribution downstream of the cascade, the loss may increase when the stagnation pressure of the coolant is taken into account. Fig. 7 shows the tip leakage loss of the cooled winglet tip. The numerical methods over predicted the losses, which is similar to the cases in Zhou and Hodson [10]. Both the experimental and numerical results show that the tip leakage loss of the cooled winglet tip increases with the coolant mass flow ratio. The effect of the coolant on the loss is smaller when the coolant mass flow rate is lower. The tip leakage loss increases notably when the coolant mass flow ratio is high. This is similar to the cases in Zhou and Hodson [10].

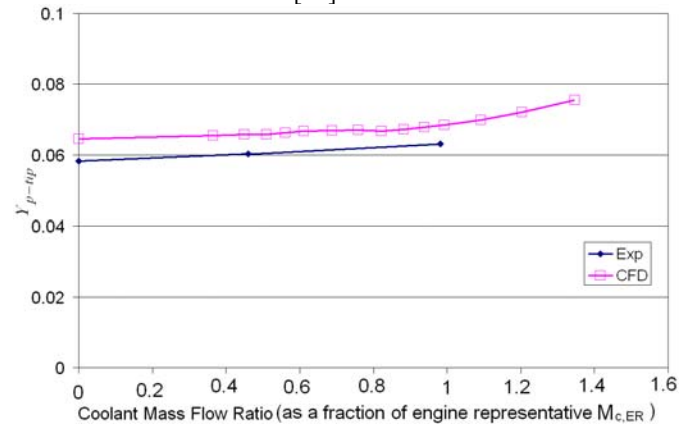


Fig. 7 Tip Leakage Loss of Cooled Tip, $\tau=1.9\%C$

In the case of a flat tip or a cavity tip, Zhou and Hodson [10] argued that the tip coolant injection affects the overall loss in four main ways. Firstly, the coolant flow is able to partially block the tip leakage flow, which reduces the tip leakage loss. Secondly, if the coolant mass flow rate is large, the coolant injection could increase the mass flow rate that exits the tip gap, which increases the loss. Thirdly, because the stagnation pressures, and therefore, the velocities of the coolant as it leaves the tip gap and the passage flow are different, losses are created as the coolant mixes with the passage flow. Finally,

losses are generated as the coolant flow enters the cooling holes from the coolant plenum. The effect of the coolant on the loss is a combination of these effects.

For this cooled winglet tip, the cooling holes are located on floor of the cavity and on the inner surfaces of the gutter. No coolant is directly injected into the tip gap from the top surface of the tip. So, the momentum exchange between the coolant and the flow that enters the tip gap from its pressure side inlet is quite small. Therefore, the reduction of the flow that enters the pressure side inlet of the tip gap is mainly achieved by the reduction of its passage area, because the tip gap is partially occupied by the coolant. At the engine representative coolant mass flow ratio, the experimental result shows that the leakage loss increases by about 6%.

THERMAL PERFORMANCE

The thermal performance of the winglet tip will be discussed for the cases of a tip gap of 1.9%C.

Cooling Effectiveness on Winglet Tip

Fig. 8 compares the experimental and numerical values of the cooling effectiveness on the winglet tip. In the experiment, the diazo films are attached to the top surfaces of the winglet tip to measure the cooling effectiveness. In general, the numerical simulation agrees with the experiment. For the area shown in the experimental results in Fig. 8(b), the average cooling effectiveness is 0.32, which is 11% higher than the CFD results. A detailed discussion will be provided in the following paragraphs.

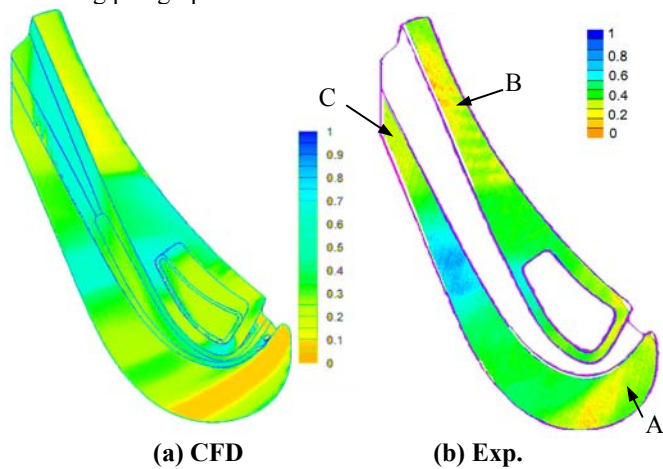


Fig. 8 Cooling Effectiveness of Cooled Winglet Tip, $M_{c,ER}$, $\tau=1.9\%C$

Fig. 9(a) shows the distribution of the cooling effectiveness around the cooling holes on the blade surface near tip region. Fig. 9(b) shows the coolant flow pathlines near the cooling holes and the cooling effectiveness on the blade surface near tip region. The colors of pathlines indicate the temperature, which is plotted using the same definition as the cooling effectiveness. On the suction side winglet, the cooling effectiveness in area '1' is satisfactory in general. The cooling effectiveness is low near the leading edge on the suction side surface because the coolant lifts off from the blade surface, as shown by the coolant

flow pathlines in Fig. 9(b). Around the three cooling holes near the leading edge as shown by '2' in Fig. 9(a), the cooling effectiveness is low because the coolant lifts off from the blade surface after exiting the cooling holes. This is indicated by the flow pathlines shown in Fig. 9(b). Although the coolant from these holes failed to cool the area around the cooling holes, it cools the top of the winglet tip.

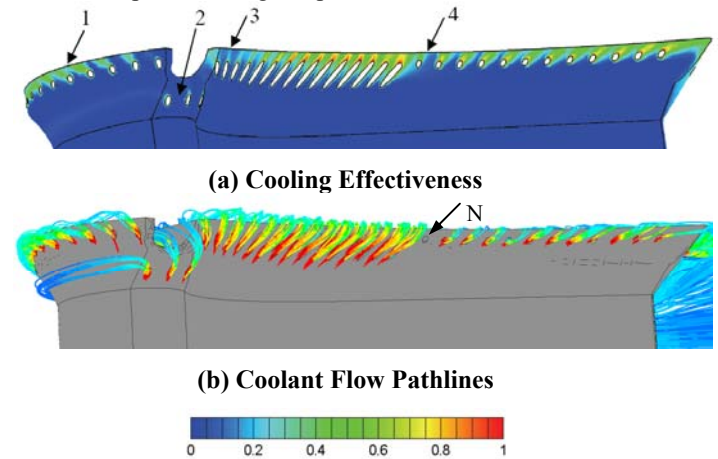


Fig. 9 Effects of Coolant on Blade Surface, $M_{c,ER}$, CFD

On the pressure side surface, the cooling effectiveness near the leading edge (area '3' in Fig. 9a) is low, mainly because the coolant does not attach on the blade surface after it exits the cooling holes. The cooling effectiveness around the hole in area '4' is much lower than that around the hole upstream of it. The main reason is that the coolant mass flow rates of the holes in area '4' are small due to the low driving pressure difference, as explained with the help of Fig. 5 in a previous section. In Fig. 9(b), no coolant pathline exits from hole 'N'. Although the CFD simulations show that some coolant exits from this hole, it is a very small amount.

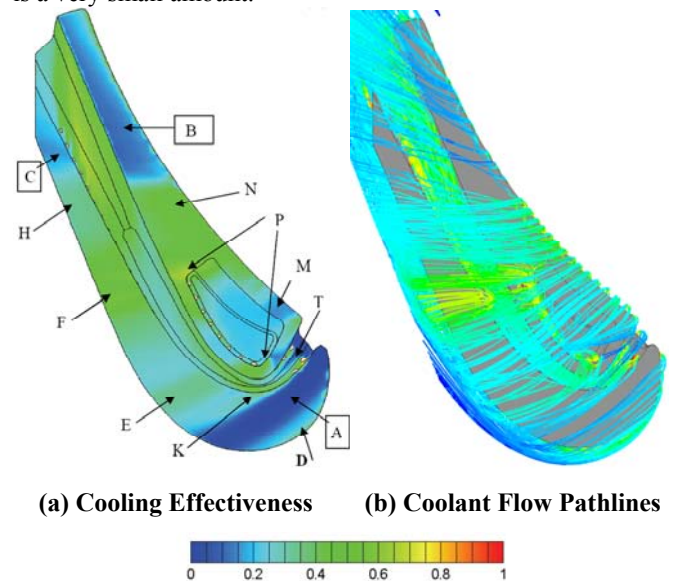


Fig. 10 Cooling Effectiveness of Cooled Winglet Tip, $M_{c,ER}$, $\tau=1.9\%C$, CFD

Fig. 10(a) shows the cooling effectiveness on the winglet tip. Fig. 10(b) shows the coolant flow pathlines over the tip. There are three main areas that are not well protected by the coolant. These are marked 'A', 'B' and 'C' in Fig. 10(a). Area 'A' is located near the leading edge of the suction side winglet. The experimental results also show that this area has low cooling effectiveness (see Fig. 8b). As shown in Fig. 10(a), part of the coolant from the suction side surface enters the tip gap and cools the area 'D' near the suction side edge of the tip, but this coolant flow can hardly cover area 'A'. Five cooling holes are located near the leading edge of the gutter (area 'T'). After the coolant exits these holes, it cools the inner surfaces of the gutter. Some of the coolant exits the gutter and covers area 'K' on the suction side winglet. However, area 'A' is located between areas 'D' and 'K', and is not well cooled.

Another area with low cooling effectiveness is located near the trailing edge of the pressure side winglet, as marked by 'B' in Fig. 10(a). The pressure side winglet is mainly cooled by the coolant ejected from the holes on the near tip pressure side surface. If the coolant mass flow rate from a hole on the pressure side surface is higher, the coolant from that hole is able to achieve higher cooling effectiveness along its trajectory over the winglet tip. The coolant mass flow rate from the holes on the pressure side surface corresponding to area 'B' in Fig. 10(a) is low, because the coolant mass flow rate is low. Therefore, the cooling effectiveness in area 'B' in Fig. 10(a) is low in this region. In the experimental results shown in Fig. 8(b), the traces of the coolant are observed in area 'B'. Each trace corresponds to the coolant that exits from a hole. These traces of the coolant are not well predicted by the CFD method, although they are visible. The main reason is that the mesh of the cooled winglet tip is not fine enough to preserve the details of such traces of the coolant. In the numerical prediction, as soon as the coolant enters the tip gap, it mixes with the leakage flow that enters the pressure side inlet of the tip gap.

In Fig. 10(a), the cooling effectiveness of area 'N' on the pressure side winglet is high, because the coolant mass flow rate is high for the cooling holes on the pressure side surface corresponding to this area. As this coolant flow travels across the tip gap, it cools the area 'H' on the suction side winglet of the tip. The cooling effectiveness is low on the small area 'M' near the leading edge, because the coolant mass flow rate from the holes on the blade pressure side is low near the leading edge of the blade as a result of the high static pressure at the exit of the cooling holes.

Near the trailing edge of the suction side winglet, the cooling effectiveness is low in area 'C' in Fig. 10(a). The suction side winglet is cooled by a combination of the coolant ejected from the pressure side surface of the blade, the cavity and the gutter. For area 'C', the coolant mass flow rate ejected from the holes near the trailing edge of the pressure side surface is low. In the gutter, after the coolant exits from the cooling holes located near the trailing edge of the gutter, it mixes with the flow inside the gutter, and mainly cools the gutter rather than the suction side winglet.

A row of cooling holes are located on the floor of the cavity near the suction side of the cavity. This coolant cools the inner surfaces of the cavity. A significant amount of the flow

inside the cavity exits the cavity from the two corners (shown by 'P' in Fig. 10(a)). As a result, the cooling effectiveness on the two corners of the cavity is high. This is also shown in the experimental result in Fig. 8(b).

On the suction side winglet, the area 'F' in Fig. 10(a) has quite high cooling effectiveness. This area is cooled by the coolant from the holes on the pressure side surface, the gutter and the cavity on the pressure side winglet. A large amount of the coolant covers this area. This agrees with the experimental result in Fig. 8(b).

The coolant that exits from the other corner of the cavity cools the area 'E' on the suction side winglet, as shown in Fig. 10(a), so the cooling effectiveness on this area is high. The cooling effectiveness between area 'E' and 'F' is lower than that on area 'E' and 'F'.

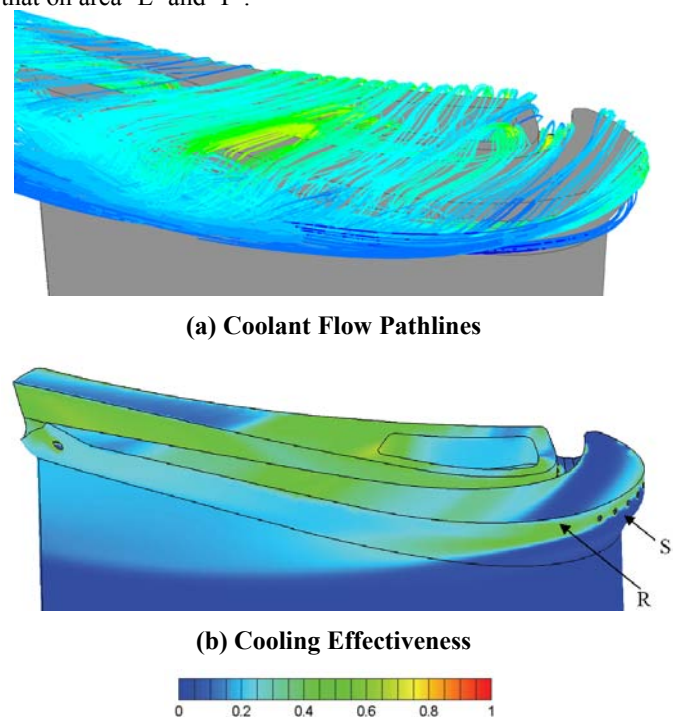


Fig. 11 Cooling Effectiveness of Blade Suction Side, $M_{c,ER}$, $\tau = 1.9\%C$, CFD

The flow pathlines in Fig. 11(a) show that after the coolant exits the tip gap, it cools the suction side of the blade surface. Fig. 11(b) shows the cooling effectiveness on the suction side of the winglet. Near the leading edge of the suction side winglet, area 'R' is effectively cooled by the coolant that exits the holes on the suction side winglet. The suction side surface of the winglet is also cooled by the coolant that exits the tip gap. However, the area 'S' is not well cooled, because no coolant covers this area.

Heat Transfer

Fig. 12 shows the distribution of the Nusselt number on the winglet tip. On the near tip region of the blade surface as shown in Fig. 12(a), the Nusselt numbers on some areas around the cooling holes are high. This is because the main passage flow

accelerates between the ejected coolant jets before entering the tip gap. Generally, these areas have low cooling effectiveness as shown in Fig. 9(a). Because of the low cooling effectiveness and high Nusselt numbers, the heat flux rates in these areas are high, resulting in poor thermal performance. Fig. 12(b) shows the Nusselt number on the top of the winglet tip. The area (e.g. area 'B') near the pressure side has high Nusselt numbers, because of the leakage flow reattachment. The area between 'C' and 'D' has low Nusselt numbers, because the cavity on the pressure side winglet reduces the leakage mass flow rate, which reduces the velocity over the area between 'C' and 'D'. The Nusselt numbers on the surface of the gutter are low, as shown in Fig. 12(b) and (c). Fig. 12(d) shows the Nusselt number on the suction side of the winglet, the tip leakage vortex impinges on the suction side surface and results in regions of high Nusselt number.

$$NHFR = \frac{q_w - q_{w,c}}{q_w} = 1 - \frac{h_c}{h_{uc}} (1 - \eta \Theta_E) \quad \text{Eq. 8}$$

where q_w is the local heat flux per unit area in the case without coolant, $q_{w,c}$ is the local heat flux per unit area in the case when the coolant is used, h_c is the heat transfer coefficient with coolant, h_{uc} is the heat transfer coefficient without coolant, η is the cooling effectiveness and Θ_E is the non-dimensional engine temperature.

$$\Theta_E = \frac{T_{01} - T_{0c}}{T_{01} - T_w} \quad \text{Eq. 9}$$

The value of Θ_E was selected as 1.5, which is the same as that used in Newton et al. [14].

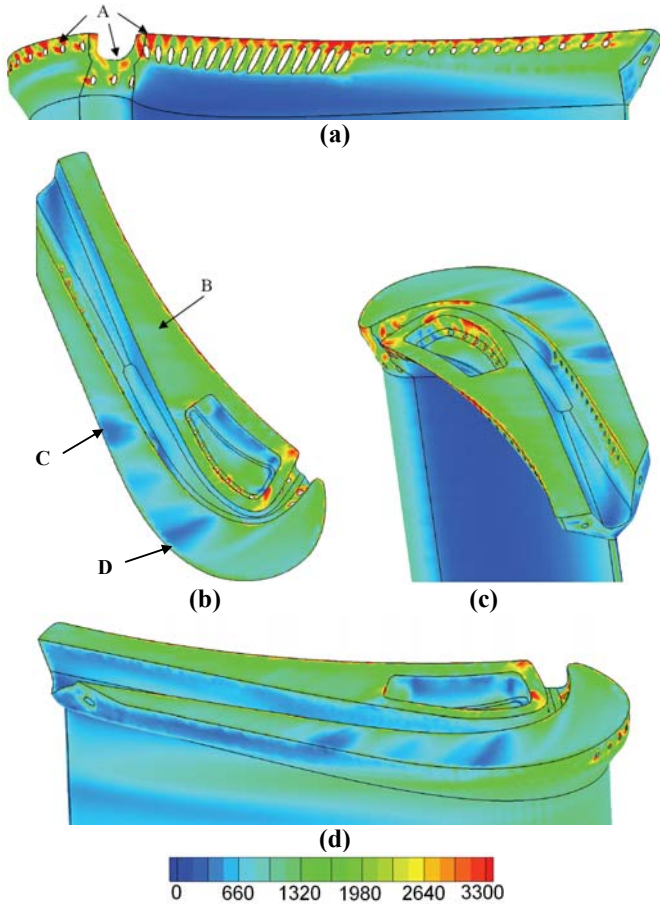


Fig. 12 Nusselt Number of Cooled Winglet Tip, $M_{c,ER}$, $\tau = 1.9\%C$, CFD

The rate of heat transfer is a combination of the cooling effectiveness and the heat transfer coefficient. In order to evaluate the combined effect, the net heat flux reduction (NHFR) is used, e.g., Newton et al. [14]. The NHFR is the ratio of the reduction in the heat flux by using the coolant to the heat flux of the case without cooling. The NHFR is defined as:

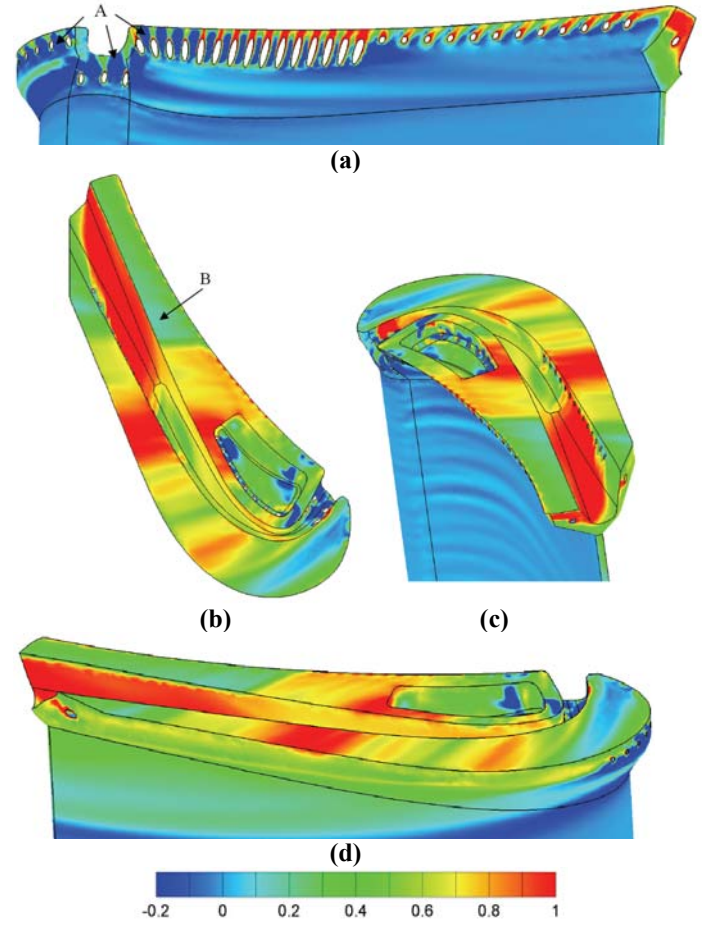


Fig. 13 NHFR of Cooled Winglet Tip, $M_{c,ER}$, $\tau = 1.9\%C$, CFD

Fig. 13 shows the distribution of the NHFR on the winglet tip. In general the NHFR is high where the cooling effectiveness is high and the NHFR is low in areas where the cooling effectiveness is low. The areas with NHFR less than zero can be critical in terms of the thermal performance, especially in areas where the heat transfer coefficients are high.

These areas appear between the coolant jets near the leading edge as marked 'A' in Fig. 13 (a).

While the NHFR represents the relative reduction of the heat flux, the heat flux rate indicates the absolute heat that enters the tip. The heat flux rate between the cooling holes in area 'A' is much higher than that on the rest parts of the blade tip. These areas may suffer from excessively high metal temperatures in a high pressure turbine. The area marked 'B' in Fig. 13(b) has low NHFR because of low cooling effectiveness. In Fig. 12(b), the Nusselt number in this area is much lower than that on area 'A' of Fig. 12(a). As a result, the heat flux rate on area 'B' in Fig. 13(b) is less than half of that in area 'A' in Fig. 13(a). The coolant mixes with the tip leakage flow and reduces its temperature. So the NHFR on the suction side surface area covered by the tip leakage flow is higher than 0, as shown in Fig. 13(d). However, areas of high Nusselt numbers appear on the suction side surface due to the tip leakage flow impingement, as shown in Fig. 12(d). As a result, the heat flux rate is not low in areas covered by the tip leakage flow impingement.

Effects of Coolant Mass Flow Ratio

The study of the winglet tip at the engine representative coolant mass flow ratio shows that the distribution of the cooling effectiveness represents well the thermal performance of the cooled winglet tip. Therefore, in this section, the distributions of the cooling effectiveness are presented to discuss the effects of the coolant mass flow ratio.

Fig. 14 shows the distribution of the cooling effectiveness around the cooling holes located on the blade surface at different coolant mass flow ratios. The coolant mass flow ratio varies from 38% to 139% of engine representative coolant mass flow ratios ($M_{c,ER}$). There are two main reasons why the cooling effectiveness around the cooling holes might be low. The first reason is that the coolant mass flow rates of the cooling holes are low. The second reason is that the coolant lifts off from the blade surface at high coolant mass flow rates.

Fig. 14(a) shows the case at 38% $M_{c,ER}$. The cooling holes are categorised into six areas 'A', 'B', 'C', 'D', 'E' and 'F'. The holes in area 'A' are located on the suction side surface of the blade. At this coolant mass flow ratio, all the holes in this area are able to provide the coolant and the cooling effectiveness around holes in area 'A' is high. In area 'B', three holes are located near the leading edge of the tip. The two holes near the blade suction side are able to provide the coolant. After the coolant exits the two cooling holes, it cools the area around it. There is no coolant injected from the holes in area 'B' near the pressure side edge, so the cooling effectiveness around this hole is low. The cooling effectiveness around area 'C' is low. In this area, the static pressures at the exit of the cooling holes are high, so the coolant mass flow rates of the cooling holes are low or no coolant exits these holes. The coolant ejected from the cooling holes around area 'D' results in good cooling effectiveness around these holes. The cooling effectiveness in area 'E' is low, because the coolant mass flow rate from these holes is low or even no coolant is ejected. This is due to the internal cooling configuration. Coolant ejected from the cooling holes in area 'F' achieves good cooling effectiveness around

these holes. Compared with the cooling holes in area 'E', the static pressure at the inlet of these coolant holes in area 'F' is higher as shown in Fig. 5, and the static pressures at the exit of the cooling holes are lower, because area 'F' is closer to the trailing edge of the blade. So, the driving pressure differences for the coolant are higher and the coolant mass flow rates are higher for cooling holes in area 'F' than that in area 'E'.

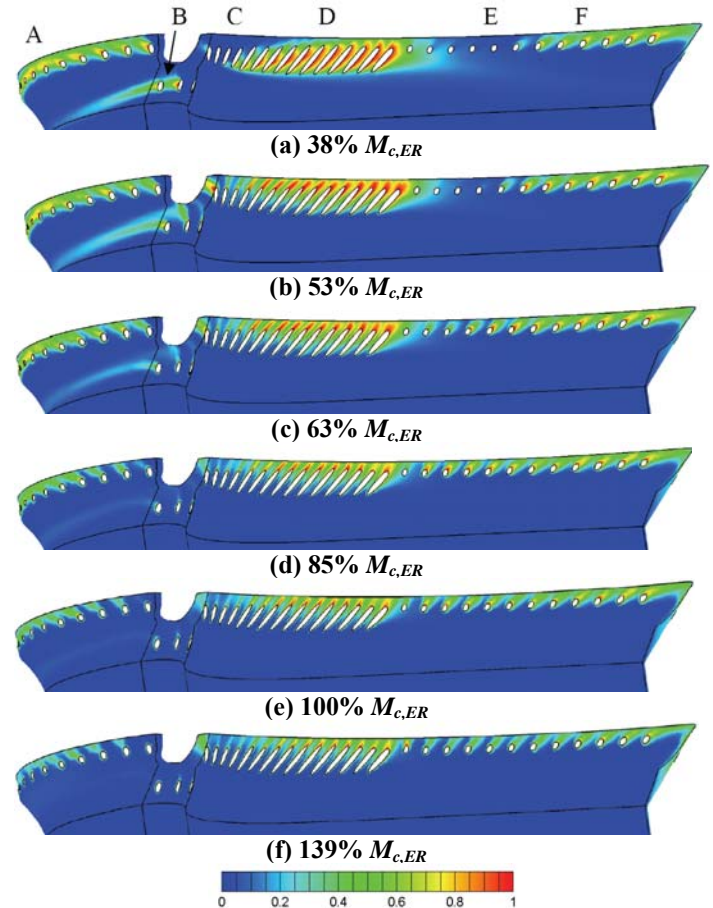


Fig. 14 Effects of Coolant Mass Flow Ratio - Cooling Effectiveness, Pressure Side Surface, $\tau = 1.9\%C$, CFD

In Fig. 14, the cooling effectiveness in area 'A' decreases when increasing the coolant mass flow ratio. This is because the coolant flow lifts off from the surface of the blade as the coolant mass flow ratio increases. At the coolant mass flow ratio of 53% $M_{c,ER}$, all the cooling holes in area 'B' are able to supply coolant. As the coolant mass flow ratio increases, the coolant flow lifts off from the surface on area 'B'. At coolant mass flow ratios larger than 85% $M_{c,ER}$, the cooling effectiveness around area 'B' is very low as little coolant attaches to the blade surface. All the cooling holes in area 'C' are able to provide the coolant at coolant mass flow ratios higher than 53% $M_{c,ER}$. As the coolant mass flow ratio increases, the cooling effectiveness around this area reduces because the coolant lifts off from the blade surface. The cooling effectiveness in area 'D' is quite good for all of the coolant mass flow ratios studied. At coolant mass flow ratios higher

than $63\% M_{c,ER}$, the cooling effectiveness of this area slightly reduces with the coolant mass flow ratio. In area 'E', all the cooling holes are able to provide coolant when the coolant mass flow ratio is higher than $63\% M_{c,ER}$. The peak value of the cooling effectiveness in area 'E' appears at the coolant mass flow ratio of $85\% M_{c,ER}$. The cooling effectiveness around the holes in area 'F' is only slightly affected by the change of the coolant mass flow ratio.

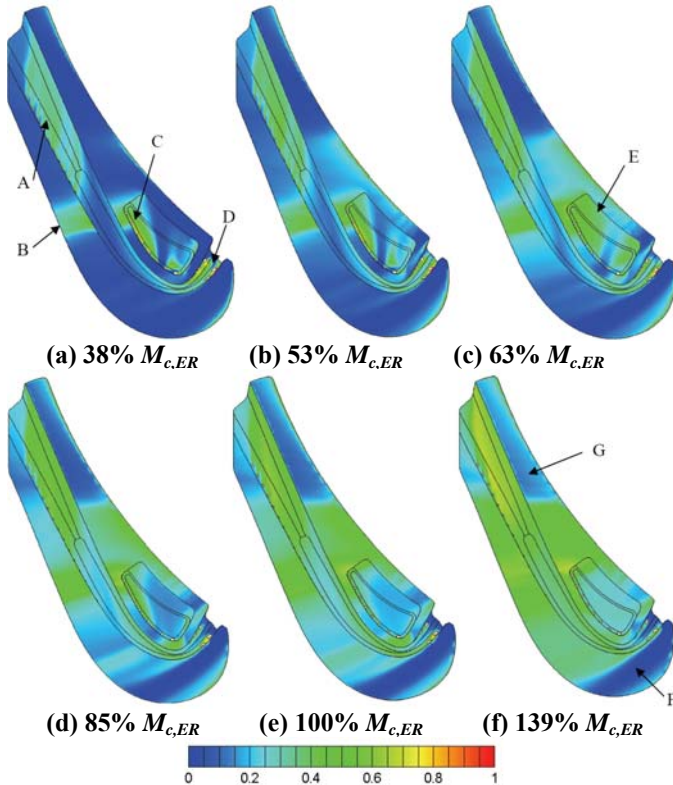


Fig. 15 Effects of Coolant Mass Flow Rate - Cooling Effectiveness, Winglet Tip, $\tau=1.9\%C$, CFD

Fig. 15 shows the distributions of the cooling effectiveness on the winglet tips at different coolant mass ratios. Fig. 15(a) shows the case when the coolant mass flow ratio is $38\% M_{c,ER}$. The area marked 'A' in Fig. 15(a) is cooled by the coolant ejected from the holes near the trailing edge of the gutter. The coolant from these cooling holes recirculates with the flow inside the gutter, covering the bottom of the gutter. The area 'B' in Fig. 15(a) has high cooling effectiveness. This area is cooled by the coolant ejected from the holes in the gutter and the coolant that exits from the cavity on the pressure side winglet. Around the cooling holes located in the cavity and near the leading edge of the gutter, the cooling effectiveness is high in areas 'C' and 'D'. In general, as the coolant mass flow ratio increases, the cooling effectiveness on the blade tip increases. One exception is the cooling effectiveness on the side and the floor of the cavity on the pressure side winglet, as shown by 'E' in Fig. 15(c). The cooling effectiveness in area 'E' is the highest at the coolant mass flow ratio of $63\% M_{c,ER}$. As the coolant mass flow ratio further increases, the coolant lifts off

from the surface of the cavity and the cooling effectiveness in this area reduces. To achieve reasonable coolant coverage on the blade tip, the coolant mass flow ratio should be larger than $85\% M_{c,ER}$. At the largest coolant mass flow ratio of $139\% M_{c,ER}$, as shown in Fig. 15(f), most areas on the blade tip can achieve good cooling effectiveness, except for the area marked 'F' near the leading edge of the suction side winglet tip. At the coolant mass flow ratio of $139\% M_{c,ER}$, the cooling effectiveness in area 'G' is quite satisfactory because the coolant mass flow rate from the holes on the blade pressure side near the trailing edge increases.

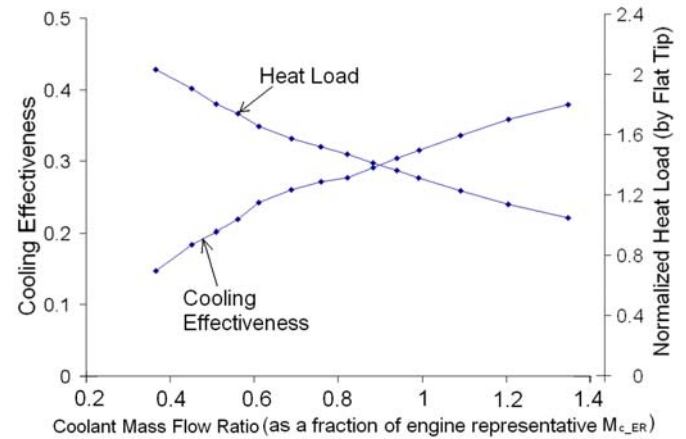


Fig. 16 Effects of Coolant Mass Flow Ratio on Thermal Performance of Cooled Winglet Tip, $\tau=1.9\%C$, CFD

Fig. 16 shows the average cooling effectiveness and the normalized overall heat flux rate on the winglet tip (not including the near tip blade surface) at various coolant mass flow ratios. As the coolant mass flow ratio increases, the cooling effectiveness on the blade tip almost increases linearly and the heat load of the tip decreases almost linearly. The winglet tip has about three times the area of a flat tip, so its heat load is quite high. At the engine representative coolant mass flow ratio, the heat load of the winglet tip is only about 1.3 times of that of an uncooled flat tip.

This means that there is a much lower average heat flux rate on the cooled winglet tip than on an uncooled flat tip. Therefore, the cooled winglet tip may require a lot of coolant air, but at the same time, it is able to survive the high gas temperatures.

EFFECTS OF RELATIVE ENDWALL MOTION

Fig. 17 shows the effects of the relative endwall motion on the cooling effectiveness on the winglet tip. Fig. 17 (a) shows the same data as Fig. 8(a). The distributions of the cooling effectiveness, which are related to the flow paths of the coolant, reflect the changes of the flow direction within the tip gap due to endwall motion. Compared to the case with the stationary endwall, the distribution of the cooling effectiveness on the winglet tip significantly changes near the leading edge of the

suction side winglet. This is because the endwall motion imposes a tangential force on the velocity of the flow near the endwall, which changes the flow pattern over the tip. With endwall motion, the tip leakage mass flow ratio reduces by about 40%, but the coolant mass flow ratio is almost unchanged. Therefore, the ratio of the coolant mass flow rate to the leakage mass flow rate increases significantly. However, less coolant from the pressure side surface of the blade enters the tip gap as the tip leakage mass flow reduces. Nevertheless, the ratio of the coolant ejected from the cavity and the gutter to the leakage flow increases. This increases the cooling effectiveness in areas such as the cavity and the gutter of the winglet tip. As a result, the average cooling effectiveness on the winglet tip increases by about 9% with endwall motion.

The effects of endwall motion have significant effects on the aero-thermal performance of the winglet tip. Details can be found in Zhou et al. [23]

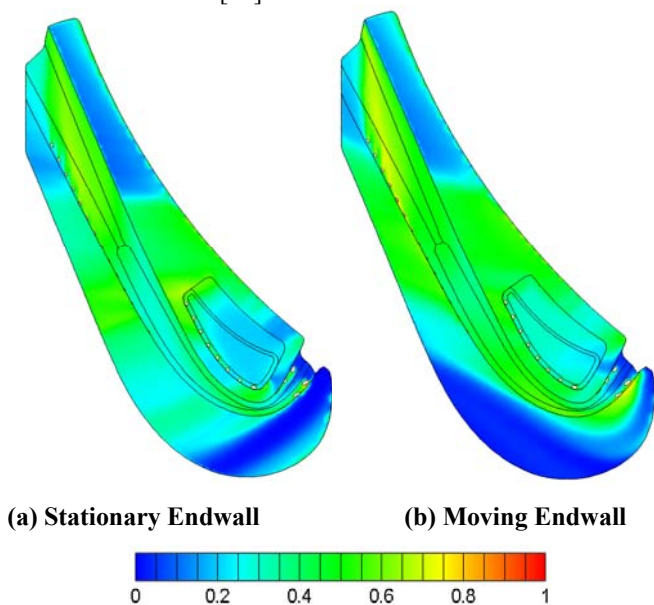


Fig. 17 Effects of Endwall Motion on the Cooling Effectiveness of Winglet Tip, CFD

CONCLUSIONS

Experimental and numerical methods were used to investigate the aero-thermal performance of a cooled winglet tip at a tip gap of 1.9%*C*.

The coolant mass flow rate of each hole varies. The coolant mass flow rate of each hole is determined by the driving pressure difference across it. The pressure at the inlet of the cooling hole is mainly determined by the stagnation pressure at the inlet of the coolant plenum and the geometry of the internal coolant configuration. The exit pressure of the cooling hole is determined by the flow field in the blade passage. The variation of the coolant mass flow rate in different cooling holes has a large impact on the thermal performance of the cooled winglet tip.

Because the coolant injection partially blocks the tip leakage flow, more passage flow is turned by the blade. As a result, the coolant injection on the winglet tip reduces the deviation of the flow downstream of the cascade due to the tip leakage flow. However, the tip leakage loss increases very slightly as the coolant mass flow rate increases. At an engine representative coolant mass flow rate, the experimental results show that the tip leakage loss increases by about 6%.

At an engine representative coolant mass flow rate, the winglet tip is cooled by the coolant ejected from the holes located on the near tip blade surface and the floor of the cavity and the gutter. On the blade pressure side surface, low cooling effectiveness appears around the holes due to the lack of the coolant from the cooling hole or the lift-off of the coolant from the blade surface when the coolant mass flow ratio is high. The cooling effectiveness is also low in areas between the coolant jets. The cooling effectiveness on the winglet tip is a combined effect of the coolant ejected from all the holes. At an engine representative coolant mass flow rate, there are three main areas on the winglet that have low cooling effectiveness due to the lack of the coolant. They are located near the leading edge of the suction side winglet, and near the trailing edge of both of the pressure side and suction side winglet. The cooling effectiveness in other areas is satisfactory.

The distribution of the cooling effectiveness represents well the thermal performance of the cooled winglet. In areas with low cooling effectiveness, the NHFR is low and the heat flux rate per unit area is normally high. The thermal performance in these areas is poor. On the near tip region of the blade surface, the NHFR is less than zero and the heat flux rate is very high between the cooling holes near the leading edge. This is because the Nusselt numbers in the areas around the cooling holes on the blade pressure side surface are high as the flow accelerates between the coolant jets into the tip gap. These are the most critical regions in terms of the thermal performance. The area near the trailing edge of the winglets also suffers from high heat flux rates, but the value is only about half of the maximum value around the holes on the pressure side surface near the leading edge. For each cooling hole on the near tip region of the surface, there is an optimum coolant mass flow ratio to achieve maximum cooling effectiveness around the hole. However, there is no optimum coolant mass flow ratio for all the holes.

On the top of the winglet tip, the average cooling effectiveness on the winglet tip increases and the heat load reduces with the coolant mass flow ratio.

ACKNOWLEDGMENTS

This work is sponsored by Rolls-Royce and the Department of Trade and Industry of UK. The authors wish to thank Rolls-Royce for the permission to publish this work.

REFERENCES

- [1] Schabowski, Z., Hodson, H., Giacche, D., and Power, B., "Aeromechanical Optimisation Of a Winglet-Squealer Tip For an Axial Turbine", GT2010-23542, 2010
- [2] Yaras, M. I., and Sjolander, S. A., "Measurements of the Effects of Winglets on Tip-Leakage Losses in a Linear Turbine Cascade". ISABE 91-7011, pp. 127-135, 1991.
- [3] Liu, H. C., Booth, T. C., and Tall, W. A., "An Application of 3-D Viscous Flow Analysis to the Design of a Low-Aspect-Ratio Turbine," ASME Paper 79-GT-53, 1979.
- [4] Harvey, N. W., "Turbine Blade Tip Design and Tip Clearance Treatment", VKI Lecture Series 2004
- [5] Dey, D., and Camci, C., "Aerodynamic Tip Desensitization of an Axial Turbine Rotor Using Tip Platform Extensions", ASME paper, 2001-GT-0484, 2001
- [6] Harvey, N., Newman, D., and Haselbach, F., "An Investigation Into a Novel Turbine Rotor Winglet. Part 1: Design and Model Rig Test Results", GT2006-90456, 2006
- [7] Papa, M., Glodstein, R. J., Gori, F., "Effects of Tip Geometry and Tip Clearance on the Mass/Heat Transfer From a Large-Scale Gas Turbine Blade", Journal of Turbomachinery, Vol.125, pp90-96, 2003.
- [8] O'Dowd, D. Zhang, Q., He, L., Oldfield, M., Ligrani, P., Cheong, B., Tibbott, I., "Aero-Thermal Performance of a Winglet at Engine Representative Mach and Reynolds Numbers", GT2010-22794, 2010
- [9] Hohlfeld, E.M., Christophel, J. R., Couch, E.L., Thole, K. A., "Predictions of Cooling From Dirt Purge Holes Along the Tip of a Turbine Blade", ASME paper GT2003-38251, 2003
- [10] Zhou, C., and Hodson, H., "The Tip Leakage Flow of an Unshrouded High Pressure Turbine Blade With Tip Cooling", ASME paper GT 2009-59637, 2009
- [11] Hofer, T., Legrand, M., Pons, L., Arts, T., "Aerodynamic Investigation of the Leakage Flow For a Blade with a Squealer Tip at Transonic Condition", 8th European Turbomachinery Conference, Graz, 2009
- [12] Hofer, T., and Arts, T., "Aerodynamic Investigation of the Tip Leakage Flow for Blades with Different Tip Squealer Geometries at Transonic Conditions", ASME paper GT2009-59909, 2009
- [13] Kim, Y. W., and Metzger, D. E., "Heat Transfer and Effectiveness on Film Cooled Turbine Blade Tip Models", Journal of Turbomachinery, Vol. 117, pp12-21, 1995b.
- [14] Newton, P. J., Lock, G. D., Krishnababu, S. K., Hodson, H.P., Dawes, W.N., Hannis, J., and Whitney, C., 2007, "Aero-thermal investigation of tip leakage flow in axial flow turbines Part III- film cooling" ASME Paper No. GT-2007-27368, 2007.
- [15] Christophel, J. R., Thole, K. A., and Cunha, F. J., "Cooling the Tip of a Turbine Blade Using Pressure Side Holes – Part 1: Adiabatic Effectiveness Measurements", Journal of Turbomachinery, Vol. 127, pp270-277, 2005
- [16] Christophel, J. R., Thole, K. A., and Cunha, F. J., "Cooling the Tip of a Turbine Blade Using Pressure Side Holes – Part 2: Heat transfer Measurements", Journal of Turbomachinery, Vol. 127, pp278-286, 2005
- [17] Ahn, J., Mhertras, S., Han, J. C., " Film-Cooling Effectiveness on a Gas Turbine Blade Tip Using Pressure-Sensitive Paint ", Journal of Turbomachinery, Vol. 127, pp.521-530, 2005.
- [18] Zhou, C., and Hodson, H., "Numerical Investigation of Thermal Performance of Unshrouded HP Turbine Blade Tips", International Journal of Turbo and Jet Engines, Vol. 26, 2009
- [19] Friedrichs, S., Hodson, H., Dawes, W.N., "Distribution of Film-cooling Effectiveness on a Turbine Endwall Measured Using the Ammonia and Diazo Technique", Journal of Turbomachinery, Vol.118, pp613-621, 1996
- [20] Zhou, C., and Hodson, H., "The aerodynamic performance of the tip leakage flow with different tip geometries", Proceedings of the 8th European Turbomachinery Conference, pp. 1469-1481, 2009
- [21] Dey, D., 2001, "Tip Desensitization in an Axial Flow Turbine", PhD thesis, The Pennsylvania State University.
- [22] Rao, N., and Camci, C., "Axial Flow Turbine Tip Desensitization by Injection from a Tip Trench. Part 1- Effect of Injection Mass Flow Rate," ASME Paper GT2004-53256 2004a.
- [23] Zhou, C., Hodson, H., Tibbott, I., Stokes, M., "Effects of Endwall Motion on the Aero-thermal Performance of a Winglet Tip in a HP Turbine" ASME paper, GT2011-46373
- [24] O'Dowd D., Zhang Q., Ligrani P., He L. and Friedrichs S. "Comparison of Heat Transfer Measurement Techniques on a Transonic Turbine Blade Tip" ASME paper, GT2009-59376, 2009.
- [25] Wheeler A. P. S., Atkins N. R., and He L. , "Turbine Blade Tip Heat Transfer in Low Speed and High Speed Flows" ASME paper, GT2009-59404, 2009.
- [26] Shadid J.N., and Eckert E.R.G., "The Mass Transfer Analogy to Heat Transfer in Fluids with Temperature-Dependent Properties" ASME Journal of Turbomachinery, Vol. 113, pp. 27-33, 1991.
- [27] Chen, G., Dawes, W. N., and Hodson, H. P. A Numerical and Experimental Investigation of Turbine Tip Gap Flow AIAA 93-2253, AIAA/SAE/ASME/ASEE, 29th Joint Propulsion Conference & Exhibit, June 28-30, 1993.